Scanning Electron Microscopy/Energy Dispersive Spectrometry Fixed-beam or Overscan X-ray Microanalysis of Particles Can Miss the Real Structure: X-ray Spectrum Image Mapping Reveals the True Nature

Dale E. Newbury and Nicholas W. M. Ritchie
National Institute of Standards and Technology, Gaithersburg, MD 20899-8370

ABSTRACT

The typical strategy for analysis of a microscopic particle by scanning electron microscopy/energy dispersive spectrometry x-ray microanalysis (SEM/EDS) is to use a fixed beam placed at the particle center or to continuously overscan to gather an "averaged" x-ray spectrum. While useful, such strategies inevitably concede any possibility of recognizing microstructure within the particle, and such fine scale structure is often critical for understanding the origins, behavior, and fate of particles. Elemental imaging by x-ray mapping has been a mainstay of SEM/EDS analytical practice for many years, but the time penalty associated with mapping with older EDS technology has discouraged its general use and reserved it more for detailed studies that justified the time investment. The emergence of the high throughput, high peak stability silicon drift detector (SDD-EDS) has enabled a more effective particle mapping strategy: "flash" x-ray spectrum image maps can now be recorded in seconds that capture the spatial distribution of major (concentration, $C > 0.1$ mass fraction) and minor ($0.01 \leq C \leq 0.1$) constituents. New SEM/SDD-EDS instrument configurations feature multiple SDDs that view the specimen from widely spaced azimuthal angles. Multiple, simultaneous measurements from different angles enable x-ray spectrometry and mapping that can minimize the strong geometric effects of particles. The NIST DTSA-II software engine is a powerful aid for quantitatively analyzing EDS spectra measured individually as well as for mapping information (available free for Java-platforms at: http://www.cstl.nist.gov/div837/837.02/epq/dtsa2/index.html).

Keywords: Elemental analysis, energy dispersive x-ray spectrometry (EDS), scanning electron microscopy (SEM), silicon drift detector - energy dispersive x-ray spectrometer (SDD-EDS), quantitative analysis, x-ray microanalysis

1. INTRODUCTION

Scanning electron microscopy/energy dispersive x-ray spectrometry (SEM/EDS) is a critical measurement technology that is widely applied in the physical and biological sciences, in engineering and manufacturing, and in forensic applications.[1] In the 2009 SPIE Scanning Microscopy symposium proceedings we presented a paper describing the impact of the newly emerging silicon drift detector energy dispersive x-ray spectrometer (SDD-EDS) on the SEM/EDS analysis of microscopic particles.[2] Compared to the previous generation of semiconductor-based energy dispersive spectrometer based upon a thick silicon crystal with resistivity compensation by lithium diffusion, Si(Li)-EDS, the thin (500 μm) wafer silicon SDD-EDS provides improved performance characteristics for all parameters of interest for microanalysis applications except for the efficiency at photon energies above approximately 10 keV. For the critical parameter of x-ray throughput [output count rate (OCR) versus input count rate (ICR)], the SDD-EDS exceeds the Si(Li)-EDS by a factor of 10 to 70 for detectors of the same active area and at the same (or better) spectral resolution. High x-ray throughput benefits all x-ray microanalysis operations by increasing the number of x-ray counts in the measured spectrum, but elemental mapping especially benefits since the act of scanning the beam to create an image effectively reduces the x-ray count per second by the number of picture elements (pixels) sampled. Moreover, the high throughput of SDD-EDS makes it particularly advantageous to collect x-ray data in the x-ray spectrum imaging (XSI) mode where a complete EDS spectrum (typically 2048 channels of 10 eV width) is collected at each pixel of an image scan. XSI measurements capture all possible information about the target region within the limitations imposed by the

Scanning Microscopies 2013: Advanced Microscopy Technologies for Defense, Homeland Security, Forensic, Life, Environmental, and Industrial Sciences, edited by Michael T. Postek, Dale E. Newbury, S. Frank Platek, Tim K. Maugel,
Proc. of SPIE Vol. 8729, 872902 · © 2013 SPIE · CCC code: 0277-786X/13/$18 · doi: 10.1117/12.2011790

physics of electron-excited x-ray generation, propagation and detection. That is, x-ray photons with a minimum energy of approximately 100 eV and a maximum energy generally limited by the incident energy, E_0, of the electron beam can be measured, enabling detection of all elements with atomic number ≥ 4 (beryllium) at concentrations, C, corresponding to major (C > 0.1 mass fraction), minor (0.01≤ C ≤ 0.1), and trace (C < 0.01) constituents, where the trace detection limit depends on the electron dose (incident beam current and detector live time), detector efficiency, and the particular element of interest and the matrix composition in which it resides.

The use of electronic Peltier cooling with passive heat transfer for operation of SDD-EDS enables implementation of detector arrangements which would have been extremely difficult or impossible with the liquid-nitrogen cooled Si(Li)-EDS. In particular, arrays of SDD-EDS now become possible. Besides the obvious improvement of increasing the total solid angle of collection and thus the geometric efficiency of measurement, having two or more SDD-EDS viewing the specimen from different azimuthal angles (where the azimuth is considered as a rotational angle around the axis of the electron beam) provides additional information which can be useful in understanding "geometric effects" on x-ray emission. These geometric effects were discussed in detail in our presentations at the 2011 and 2012 SPIE Scanning Microscopy symposia and will only be summarized here:[3,4] Relative to a flat surface (1) electron scattering from a tilted surface produces higher backscattering and a larger fraction of high energy backscattered electrons (BSE), both of which reduce the production of x-rays at all photon energies, but the loss of BSEs with higher energy especially impacts production of higher photon energies, E > 4 keV; (2) the depth of penetration into a tilted target averaged over all of the incident beam electrons is reduced because of the enhanced loss of BSEs; as a result, x-rays are produced at shallower depths which favors the escape of low energy photons, E < 4 keV, compared to a flat target at normal beam incidence; (3) because of variations in the local specimen topography, the x-ray escape path to the detector can be greater or lesser than the case for a flat specimen, and since x-ray absorption follows an exponential dependence on the path length, these path length variations can have an especially strong impact on the efficiency of escape, particularly affecting the low energy photons that are subject to high absorption.

Particle analysis is vulnerable to geometric effects because of the local surface curvature, which causes significant variations in the spectrum measured from a compositionally-homogeneous particle depending on the placement of the electron beam. As shown in Figure 1 for the case of a large spherical particle, where "large" refers to a particle diameter that is at least a factor of ten greater than interaction volume for that composition and incident beam energy, the effective path length to the x-ray detector depends strongly on the beam position on the particle relative to the EDS. For a beam placed at the top center of a large particle, the surface curvature is so small that the interaction volume and x-ray path length are similar to what they would be for an ideal flat surface. However, when the beam is placed on the side of the particle toward or away from the detector, the local surface curvature significantly changes the effective absorption path length. When the beam is placed on the side of the particle toward the x-ray detector, the interaction volume is effectively that of a highly tilted surface with the x-ray detector viewing along a take-off angle approaching 90°, which gives the shortest possible absorption path. Relative to the x-ray spectrum measured at the top center position, this short absorption path results in greater escape for the low energy photons. In the spectra shown in Figure 1 for a 20 μm-diameter particle of alloy IN100, whose composition is listed in Table 1, the intensity for AlK (1.487 keV) is approximately 40% higher compared to the AlK intensity measured with the beam placed at the particle top center. When the beam is placed on the side of the particle away from the x-ray detector, the interaction volume is again that appropriate to a highly tilted surface, but to reach the EDS the x-rays now must pass back through almost the full diameter of the particle. This extended path is shown schematically as the dashed magenta arrow in Figure 1. The consequence to the spectrum (red trace) is a preferential loss of low energy photons. For the AlK peak, about 60% of the intensity is lost compared to the spectrum measured at the top center of the particle. The effects of the particle geometry on quantitative analysis thus depend on the exact beam location. Depending on where the measurement takes place, elements measured with low energy photons will be overrepresented or underrepresented relative to elements measured with high energy photons. An example is given in Table 1 for an 80 μm-diameter particle of alloy IN100, which shows these significant geometric effects on quantitative analysis, as indicated by the sharp drop in the analytical total on the side away from the EDS, a total of 0.76 compared to 0.98 at the top center.

SDD-EDS detector arrays provide multiple views of the specimen that can aid in interpreting particle geometry effects and minimizing their impact on x-ray microanalysis by selecting the optimum view of a specimen with complex topography or by combining spectra measured from different angles to reduce the effects of self-screening.

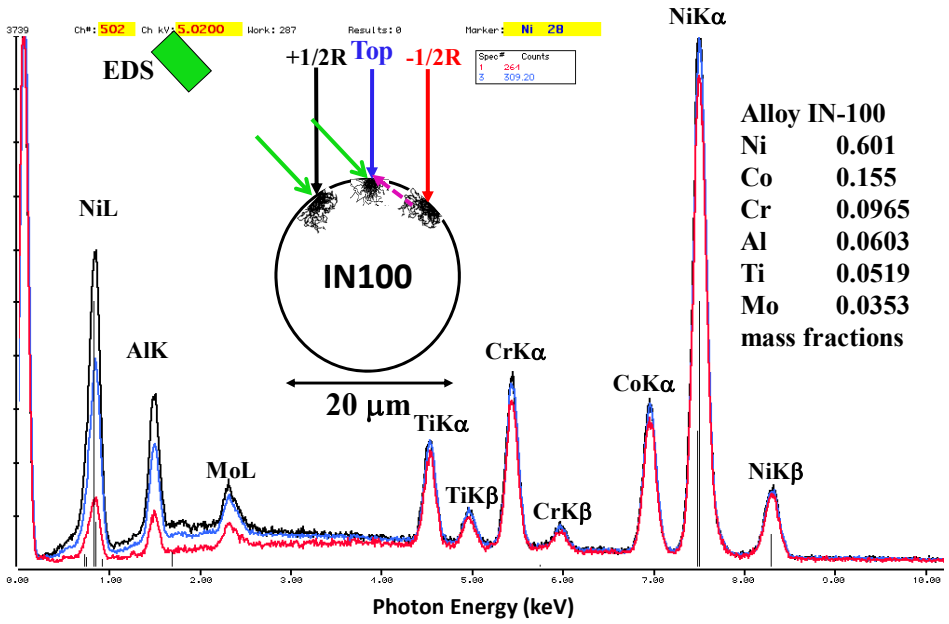

Figure 1. Schematic diagram of x-ray generation and propagation with the beam placed at three locations on a particle of alloy IN100 and measured EDS spectra corresponding to the three locations noted.

Table 1 Alloy IN-100 bulk composition; point and overscan analyses of 80 µm-diameter particle

Element	Alloy bulk comp mass fraction specification; **xsec analyzed**	Particle, location toward EDS; raw mass conc **normalized conc**	Particle, center; raw mass conc **normalized conc**	Particle, location away from EDS; raw mass conc **normalized conc**	Bracketing overscan; raw mass conc; **normalized conc**
Al	0.05 to 0.06 **0.0603 ± 0.0001**	0.0736 ± 0.0001 **0.0747 ± 0.0001**	0.0459 ± 0.0001 **0.0469 ± 0.0001**	0.0089 ± 0.0001 **0.0117 ± 0.0001**	0.0192 ± 0.0001 **0.0356 ± 0.0001**
Ti	0.045 to 0.055 **0.0519± 0.0001**	0.0413 ± 0.0001 **0.0419 ± 0.0001**	0.0569 ± 0.0001 **0.0581 ± 0.0001**	0.0287 ± 0.0001 **0.0379 ± 0.0001**	0.0275 ± 0.0001 **0.0510 ± 0.0001**
Cr	0.08 to 0.11 **0.0965± 0.0003**	0.0960 ± 0.0001 **0.0974 ± 0.0001**	0.0958 ± 0.0001 **0.0978 ± 0.0001**	0.0695 ± 0.0001 **0.0917 ± 0.0001**	0.0483 ± 0.0001 **0.0895 ± 0.0003**
Co	0.13 to 0.17 **0.155± 0.0005**	0.1506 ± 0.0002 **0.1528 ± 0.0002**	0.1481 ± 0.0002 **0.1512 ± 0.0002**	0.1262 ± 0.0002 **0.1666 ± 0.0002**	0.0837 ± 0.0002 **0.1552 ± 0.0006**
Ni	0.565 to 0.675 **0.601± 0.0010**	0.5903 ± 0.0005 **0.5990 ± 0.0005**	0.6030 ± 0.0005 **0.6158 ± 0.0005**	0.5150 ± 0.0005 **0.6799 ± 0.0005**	0.3459 ± 0.0004 **0.6410 ± 0.0017**
Mo	0.02 to 0.04 **0.0353± 0.0002**	0.0336 ± 0.0002 **0.0341 ± 0.0002**	0.0296 ± 0.0001 **0.0302 ± 0.0001**	0.0093 ± 0.0001 **0.0123 ± 0.0001**	0.0149 ± 0.0001 **0.0277 ± 0.0002**
Analyzed sum		0.9854 ± 0.0012	0.9792 ± 0.0012	0.7575 ± 0.0010	0.5396 ± 0.0009

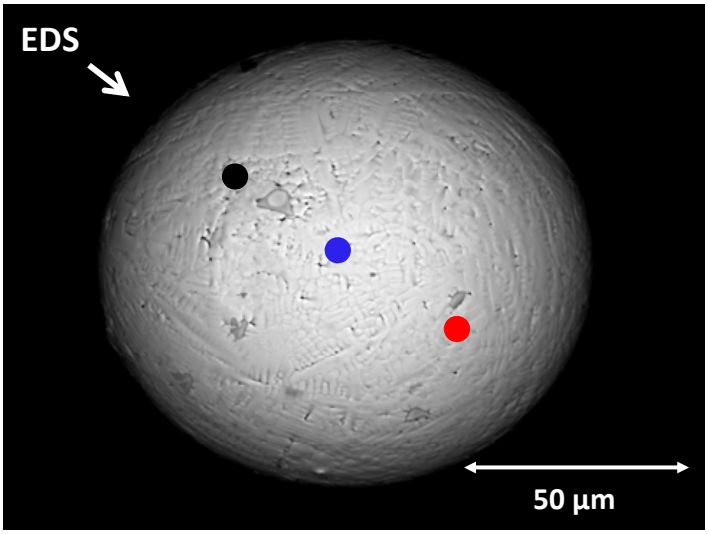

Figure 2. Particle of alloy IN100. Dots mark locations of analyses reported in Table 1.

2. EXPERIMENTAL DETAILS*

Measurements were performed with two different SEM/SDD-EDS systems:
1. JEOL thermal field emission gun scanning electron microscope (tFEG-SEM) equipped with a Bruker QUAD SDD-EDS consisting of four 10 mm^2 detectors, co-mounted and located at a distance of 72 mm from the beam impact point on the optic axis. The solid angle of collection was 0.0077 sr and the take-off angle was 40° above the surface. The outputs of all detectors were combined for all measurements. Data were collected in the x-ray spectrum image mode using the Bruker software and the maps were exported in the RAW file format for subsequent detailed analysis with the NIST image processing engine Lispix (available free at: http://www.nist.gov/lispix/) and with the NIST EDS software engine DTSA-II (available free at: http://www.cstl.nist.gov/div837/837.02/epq/dtsa2/index.html)[5, 6].
2. TESCAN tFEG-SEM equipped with four separate 30 mm^2 PulseTor SDD-EDS detectors at a distance of 32 mm from the beam impact on the specimen, giving a solid angle of 0.029 sr for the individual detectors and a total solid angle of 0.117 sr for the combined signal. The detectors were mounted around the optic axis of the instrument with separations of approximately 90 degrees. The measured x-ray signals could be combined or examined individually, which because of the four discrete viewing angles represented has advantages with specimens that feature irregular topography. Data were collected with a custom software system based upon NIST DTSA-II.

Particle samples were prepared by attachment to a conducting carbon tape substrate and carbon coating (~ 10 nm) by thermal evaporation to provide a conducting path to discharge insulating specimens. Particle sources included NIST reference materials, commercial alloys, and environmental samples.

*Disclaimer

Certain commercial equipment, instruments, or materials are identified in this paper to foster understanding. Such identification does not imply recommendation or endorsement by the National Institute of Standards and Technology, nor does it imply that the materials or equipment identified are necessarily the best available for the purpose.

3. RESULTS

Mapping from a single detector direction: Figures 3(a) and 3(b) show the backscattered electron (BSE) image, elemental maps (background-corrected x-ray intensity) for Al, Ti, Cr, Co, Ni, and Mo, and a color superposition image with Mo = red, Ti = green, and Ni = blue of a 200 µm-diameter spherical particle of the alloy IN-100 obtained with instrument configuration 1. The XSI scan was 512 pixels by 384 pixels with a pixel dwell of 1024 µs for a total collection time of 201 s. Mapping reveals that this particle is heterogeneous on a coarse scale with Ti-Mo-rich inclusions in an apparently homogeneous matrix of Al, Cr, Co, and Ni. However, the Ti image also reveals the structure of the solidification dendrites which form an extensive filigree-like pattern throughout the matrix of the particle, showing a micrometer-scale level of Ti heterogeneity. This heterogeneity is one reason for the deviation of the measured composition at the top center location on the particle from the ideal batch composition. As a consequence of the topography of the particle, which causes the systematic variations in the x-ray intensities in the spectra measured at various locations in Figure 1, elemental x-ray maps feature strong shadows created on the side of the particle away from the SDD-EDS detector, which views the specimen from the direction indicated in Figure 3(b) at an elevation angle of 40° above the horizontal (50° from the incident electron beam). For the x-ray maps, the particle appears to be illuminated from the direction of the x-ray detector, which is asymmetrically placed. By comparison, the BSE image in Figure 3(a) appears evenly illuminated because the BSE detector is annular and placed symmetrically around the incident beam so that the source of illumination appears to be along the line-of-sight (i.e., the electron beam).

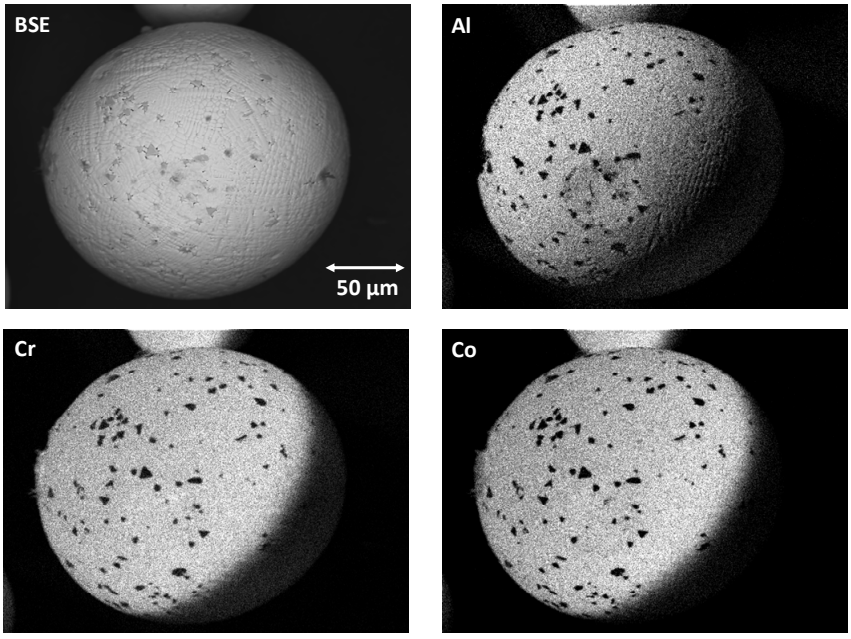

Figure 3(a) Particle of alloy IN100: BSE image; x-ray intensity maps for Al (K-$L_{2,3}$), Cr (K-L_3), and Co (K-L_3).

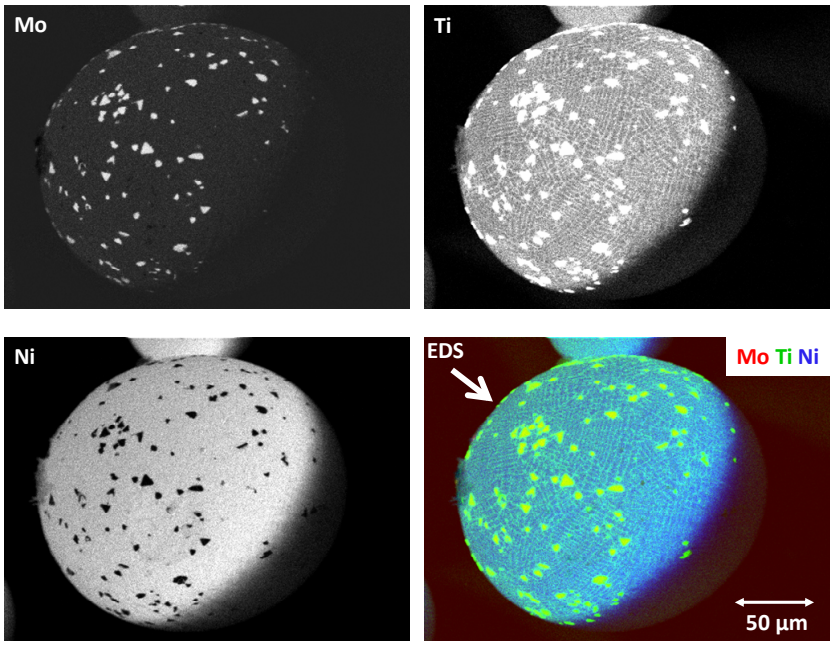

Figure 3(b) Particle of alloy IN100: x-ray intensity maps for Mo ($L_{2,3}$-$M_{4,5}$), Ti (K-L_3), and Ni (K-L_3), and a color superposition with Mo = red, Ti = green, and Ni = blue.

Mapping with multiple SDD-EDS detectors to get the best picture: By having a symmetric array of SDD-EDS detectors surrounding the beam, the problem of topographic screening of an individual detector is greatly reduced. Figure 4 shows an example of mapping a particle of IN100 alloy with a single SDD-EDS and with an array of four SDD-EDS. This x-ray spectrum image data was collected simultaneously from all four SDD-EDS detectors, and the single detector data was selected as a subset from the full XSI. The geometric screening observed in the example of Figure 3 from a single detector is almost completely eliminated with the array of four SDD-EDS viewing the specimen from the directions indicated. In addition to the elemental images for Ni and Ti, Figure 4 also contains maps based upon the analytical total, which is the sum of all of the constituents at each pixel. Examining the analytical total image provides insight into the particle topographic effects. The Analytical Total image for the single SDD-EDS shows the complete loss of information on the side of the spherical particle opposite to the single detector, which occurs due to severe x-ray absorption along the extended paths through the particle to reach the detector, as explained in Figure 1. The SDD-EDS array shows a much more uniform Analytical Total image. However, subtle geometric effects still occur due to the particle topography even with four SDD-EDS collecting the x-rays. Close examination reveals a large region of nearly uniform intensity on the top of the particle where the analytical total is at or near the maximum, but on the rounded sides of the particle, the analytical total diminishes relative to the top. While the array of SDD-EDS detectors eliminates the strong effects of absorption shadowing, the decrease in the analytical total observed on the sides of the particle results from enhanced electron backscattering as the particle curvature effectively increases the local sample inclination to the beam. The total x-ray production decreases due to the increased loss of high energy backscattered electrons.

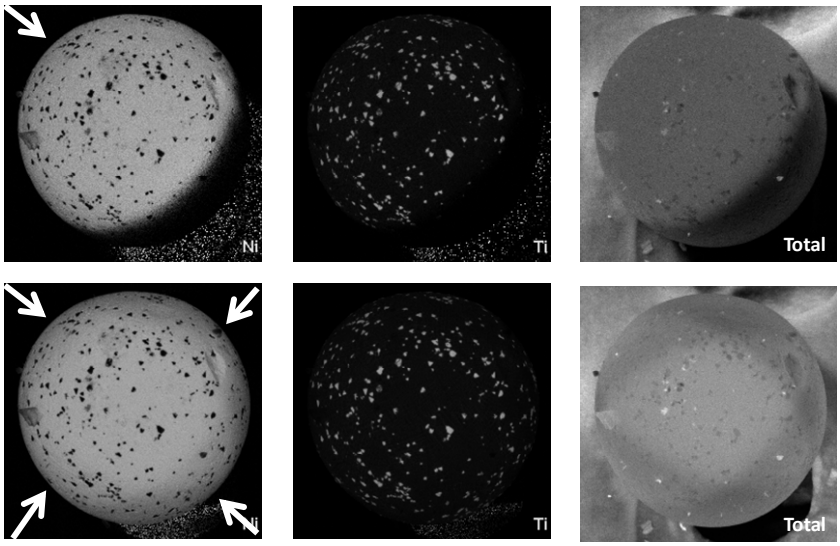

Figure 4 Particle of alloy IN100 mapped with an array of four SDD-EDS, comparing the geometrical screening with a single SDD-EDS (viewing the specimen from the upper left) and with all four SDD-EDS. In addition to Ni (K-L_3)and Ti (K-L_3) elemental maps, the Analytical Total map is also compared.

Application

Environmental particles: Figure 5 shows an example of a map of a complex particle aggregate found in the fly ash of a coal-fired power plant. The SEM secondary electron (SE) image reveals the complex topography of the aggregate particle, and the SEM backscattered electron (BSE) image, which is sensitive to compositional differences, shows contrast that indicates that the aggregate particle has distinct compositional substructure. However, the information provided by the x-ray spectrum image is needed to fully understand the complex nature of the particle. The bright regions observed in the SEM-BSE image are seen to correspond to Fe-enrichment. However, the XSI reveals compositional features that are not apparent in the SEM-BSE image because they consist of elements that are relatively close in atomic number. As indicated in the Ca map, there are two spherical regions, labeled "1" and "2", that appear black, and which do not correspond to Fe-enrichment, as seen in the color overlay of Si, Fe, and Ca. Using the spectrum sampling tools available for the XSI, spectra of these two regions indicate a high Al content, and when the Al map is derived from the XSI, the Al-rich particles are revealed. Examining the SEM-SE image reveals that both spherical Al-rich particles "1" and "2" are surface decorations of the aggregate particle, but in the SEM-BSE image, Al-rich particle "2" is nearly invisible due to a close match in average atomic number with the surrounding matrix of the aggregate particle. Finally using the Maximum Pixel spectrum, the presence of a S-rich inclusion is recognized.

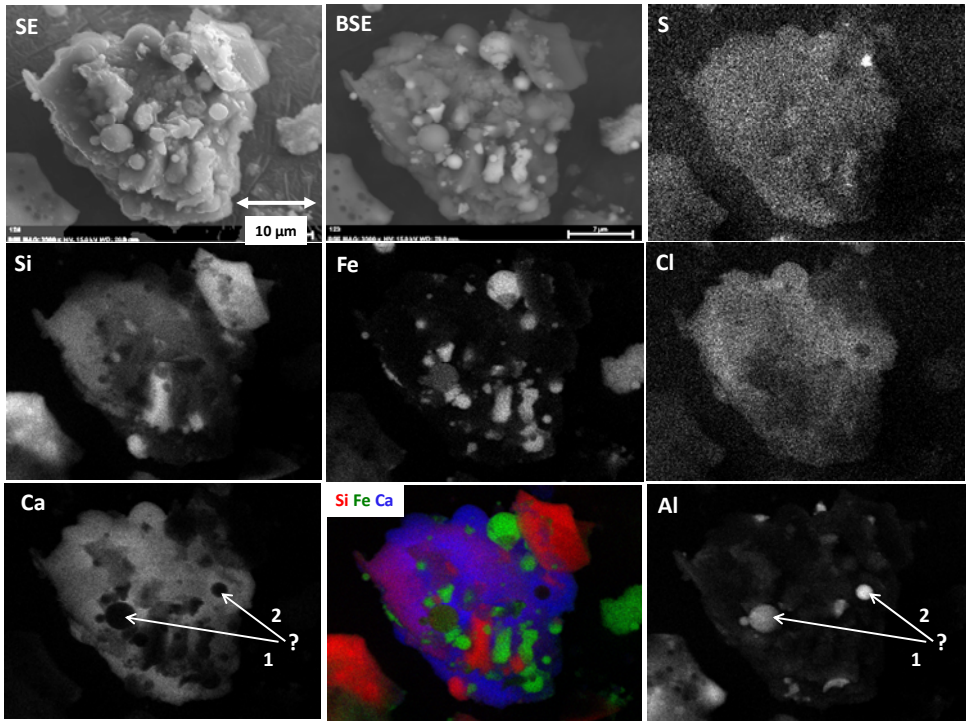

Figure 5. Application of x-ray spectrum imaging to elucidate the complex elemental microstructure of a particle aggregate from the fly ash of a coal-fired power plant (sample courtesy of John Small, NIST). SEM "secondary electron" image with the Everhart-Thornley detector; SEM BSE image; x-ray elemental maps for S (K-$L_{2,3}$); Si (K-$L_{2,3}$); Fe (K-L_3); Cl (K-L_3); Ca (K-L_3); Al (K-$L_{2,3}$); color overlay with Si (red); Fe (green); Ca (blue).

4. DISCUSSION

For more than 40 years, SEM/EDS analysis has provided a powerful technique capable of solving problems which require understanding the nature of elemental distributions at the microstructural level. As with all spectrometric measurement techniques, the performance has been ultimately limited by the available detector technology. In the case of EDS measurements, the critical issue is the number of x-rays that can be measured per unit time and per unit of electron dose delivered to the specimen. Compared to the older Si(Li)-EDS technology, SDD-EDS provides greatly enhanced x-ray throughput, which reduces the measurement time to achieve a specific level of precision when electron dose is not an issue, and enables implementation of individual detectors of large solid angle as well as arrays of detectors, which lowers the electron dose necessary to achieve a specified level of precision or detection sensitivity. Important parallel advancement has occurred in the SEM platform through implementation of the thermal field emission gun (tFEG), which provides the high, stable beam current in a small focused probe needed to fully exploit the advantages of SDD-EDS. The combination of tFEG-SEM and SDD-EDS provides the microscopist/microanalyst with a tool that offers remarkably improved performance in both imaging and x-ray microanalysis, so much so that it is appropriate to consider new strategies for applying the method. While older techniques still have merit, it is time to apply strategies that always collect the maximum available data about a region. Thus, data collection in the x-ray spectrum imaging mode should be utilized whenever the heterogeneity of the specimen is an important question. Considering that many objects are heterogeneous on a microstructural scale, SDD-EDS XSI operation is likely to reveal significant information that past measurement strategies tended to overlook due to the measurement limits imposed by EDS performance. SDD-EDS constitutes a "sea change" in capabilities, and calls for serious reconsideration of the ways in which the SEM/EDS technique is applied.

5. REFERENCES

Contribution of the United States Government not subject to copyright protection within the United States.

[1] Goldstein, J., Newbury, D., Joy, D., Lyman, C., Echlin, P., Lifshin, E., Sawyer, L., and Michael, J., [Scanning Electron Microscopy and X-ray Microanalysis, 3rd edition], Springer, New York, 462-470 (2003).
[2] Newbury, D. Ritchie, N. and Bright, D., "Characterizing Heterogeneous Particles with SEM/SDD-EDS Mapping and NIST Lispix" Scanning Microscopy 2009, Proc. SPIE 7378, Q1-Q11 (2009).
[3] Newbury, D. and Ritchie, N. "Is Scanning Electron Microscopy/Energy Dispersive X-ray Spectrometry (SEM/EDS) Quantitative? Effects of Specimen Shape" Proc. SPIE. 8036, 803602-1 - 803602-16 (2011).
[4] Newbury, D. and Ritchie, N., "Faults and Foibles of Quantitative Scanning Electron Microscopy/Energy Dispersive X-ray Spectrometry (SEM/EDS), Proc. SPIE. 8378, 837803-1 to 837803-12 (2012).
[5] Bright, D., "Lispix: a software engine for spectrum image processing," available for free download at: http://www.nist.gov/lispix/.
[6] Ritchie, N., "Getting Started with NIST DTSA-II", Microscopy Today, (19) 2011 26-31; DTSA-II is available for free download at www.cstl.nist.gov/div837/837.02/epq/dtsa2/index.html.